ARL-CR-0879 ● Nov 2024

Review of Neuromodulation Effects Due to Acoustic and Thermoacoustic Signals

prepared by Rebecca Laher and Robert Haupt
Massachusetts Institute of Technology Lincoln Laboratory
244 Wood St
Lexington, MA 02421

under contract FA870215-D-0001

NOTICES

Disclaimers

The findings in this report are not to be construed as an official Department of the Army position unless so designated by other authorized documents.

Citation of manufacturer's or trade names does not constitute an official endorsement or approval of the use thereof.

Destroy this report when it is no longer needed. Do not return it to the originator.

ARL-CR-0879 ● Nov 2024

Review of Neuromodulation Effects Due to Acoustic and Thermoacoustic Signals

prepared by Rebecca Laher and Robert Haupt
Massachusetts Institute of Technology Lincoln Laboratory
244 Wood St
Lexington, MA 02421

under contract FA870215-D-0001

REPORT DOCUMENTATION PAGE

1. REPORT DATE	2. REPORT TYPE	3. DATES COVERED	
		START DATE	END DATE
November 2024	Contractor Report	2/01/2023	2/28/2024

4. TITLE AND SUBTITLE
Review of Neuromodulation Effects Due to Acoustic and Thermoacoustic Signals

5a. CONTRACT NUMBER	5b. GRANT NUMBER	5c. PROGRAM ELEMENT NUMBER
FA870215-D-0001		
5d. PROJECT NUMBER	**5e. TASK NUMBER**	**5f. WORK UNIT NUMBER**
3714		

6. AUTHOR(S)
Rebecca Laher and Robert Haupt

7. PERFORMING ORGANIZATION NAME(S) AND ADDRESS(ES)
Massachusetts Institute of Technology Lincoln Laboratory
244 Wood St
Lexington, MA 02421

8. PERFORMING ORGANIZATION REPORT NUMBER

9. SPONSORING/MONITORING AGENCY NAME(S) AND ADDRESS(ES)	10. SPONSOR/MONITOR'S ACRONYM(S)	11. SPONSOR/MONITOR'S REPORT NUMBER(S)
DEVCOM Army Research Laboratory ATTN: FCDD-RLA-HC Aberdeen Proving Ground, MD 21005		ARL-CR-0879

12. DISTRIBUTION/AVAILABILITY STATEMENT
DISTRIBUTION STATEMENT A. Approved for public release: distribution unlimited.

13. SUPPLEMENTARY NOTES
ORCIDs: Rebecca Laher, 0000-0002-8786-5191; Robert Haupt, 000-0003-3385-7601

14. ABSTRACT
Recent efforts in the medical and defense fields aim to better understand how ultrasound modulates brain function. This report explores neuromodulation effects from acoustic signals in the brain originating from various sources, including a literature review of what is known from ultrasound applied transcranially via contact transducers. One way of applying ultrasound is with an RF source via the thermoacoustic effect. We explore the RF source parameters required to generate comparable levels of ultrasound in the brain as is generated via contact transducers for neuromodulation. Source carrier frequencies between 1 and 10 GHz are considered. Focusing effects of ultrasound at depth are also explored, suggesting the necessary peak RF powers could be of similar magnitude to the Institute of Electrical and Electronics Engineers safety standard given the right circumstances. This analysis assumes single pulses of RF that absorb in the neural tissue to generate ultrasound pressure waves. Further analysis is required to explore cumulative pulsing effects or generation of ultrasound in surface layers (e.g., the skull) and then traveling into the brain mass.

15. SUBJECT TERMS
thermoacoustics, RF, ultrasound, neuromodulation, transcranial focused ultrasound, Biological and Biotechnology Sciences

16. SECURITY CLASSIFICATION OF:			17. LIMITATION OF ABSTRACT	18. NUMBER OF PAGES
a. REPORT	b. ABSTRACT	C. THIS PAGE		
UNCLASSIFIED	UNCLASSIFIED	UNCLASSIFIED	UU	32

19a. NAME OF RESPONSIBLE PERSON	19b. PHONE NUMBER *(Include area code)*
Amy Dagro	(410) 278-3889

STANDARD FORM 298 (REV. 5/2020)
Prescribed by ANSI Std. Z39.18

Contents

List of Figures

List of Tables

1. Introduction

This report is intended to review the bioeffects that acoustic and thermoacoustic signals have on the electrophysiological function of the brain. Noninvasive brain stimulation techniques are currently being researched in the medical and defense communities to understand mechanisms that initiate and modulate neural activity affecting brain function. It is proposed that if these energy forms can be focused in regions of the brain and optimized, then noninvasive methods may have potential to administer therapies that could modify and reverse a variety of brain function disorders. The present report first discusses the current understanding of neural interactions in the healthy brain and limitations to this model. The impact that each of the above energy forms has on the brain, including proposed mechanisms of action and how neural response may vary due to severity, frequency, and location of impact, will be evaluated through supporting evidence from the literature.

1.1 Review of Neuron Anatomy and Physiology

The nervous system is highly complex and not yet fully understood by the scientific community. This section discusses the current working model of how neurons interact through electrochemical signaling as proposed by researchers Hodgkin and Huxley (1952). Limitations to the Hodgkin–Huxley model discovered over the years may provide insight to how other signals (e.g., mechanical) modify neural behavior.

There are approximately 86 billion neurons in the central nervous system (CNS), all with varying structures, functions, gating mechanisms, and thresholds of activation. A simplified depiction of a neuron is shown in Figure 1 and can be broken down into four main structural components: the dendrites, which receive signals; the soma, where the nucleus and other cell organelles are located; the axon, along which electrochemical signals propagate; and the synaptic terminal, where vesicles containing neurotransmitters are stored. When an electrochemical signal transmits all the way to the synaptic terminal, neurotransmitters are released into the extracellular space to bind to receptors on the dendrites of other neurons. Neurons throughout the brain store varying types of neurotransmitters that result in differing responses to neurons downstream. For example, gamma-aminobutyric acid is a common neurotransmitter known to have an inhibitory effect on neurons, whereas the neurotransmitter glutamate has an excitatory effect on neurons. If an inhibitory behavior is observed in response to an energy source, that result could be due to either an inhibition of excitatory neurons or to an excitation of inhibitory neurons. It is therefore critical when discussing the effects of neuromodulation on

a particular group of neurons to consider which region of the brain is being targeted and the various functions of the neurons that will be impacted.

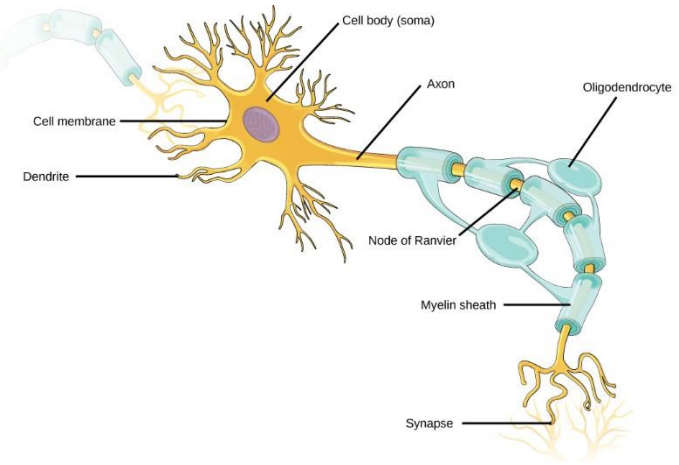

Figure 1. Simplified neuron.

An electrochemical signal in neurons is defined as the local change of the voltage across the cell membrane due to a flux of ions into or out of the cell. A typical neuron at rest has an intracellular voltage of –70 mV with an ion distribution as detailed in Table 1. Ion flux across the membrane can occur actively via pumps or passively through channels where ions will travel down their concentration gradient into or out of the cell. Ion channels are proteins embedded in the cell membrane that can vary in gating mechanism, sensitivity, and ion specificity.

Table 1. Ion concentration in neurons at rest gives a membrane potential of approximately −70 mV (Liberman and Adams 2005).

Ion	Intracellular (mM)	Extracellular (mM)
Sodium (Na^{+})	10	140
Potassium (K^{+})	150	5
Calcium (Ca^{2+})	0.0001	1.2
Chloride (Cl^{-})	30	120

Some common channel gating mechanisms are chemical, voltage, and mechanical. Chemically gated channels have receptors where ligands such as ions or neurotransmitters can bind, resulting in a conformational change to the protein structure that opens the channel and allows ions to flow. Voltage-gated ion channels have a subunit made up of positively charged amino acids such as lysine and arginine. A buildup of positively charged ions on either side of the cell will repel the subunit into either the open or closed configuration. Mechanically gated ion channels can open due to a transfer of momentum or increased mechanical stress on the cell membrane, resulting in the channel being physically pulled open. The classic electrochemical understanding of neuronal activity described by Hodgkin

and Huxley (1952) includes the involvement of chemically gated and voltage-gated ion channels, but it does not consider any thermodynamic or mechanical stimuli that may activate neurons. This is discussed further in Section 2.1, where the potential mechanisms of activation of neurons via acoustic signal in the CNS are reviewed.

A neuron's dendrites can receive both excitatory and inhibitory signals, as shown in Figure 2. A neuron will fire if the cumulative effect of all signals received by the cell exceeds the voltage activation threshold, resulting in a regenerative positive membrane potential traveling the entire length of the axon down to the axon terminal. This transmitted positive signal along the axon is referred to as an "action potential" and typically occurs at an activation threshold of about –10 mV, although both the resting voltage and activation threshold can vary across neuron types. An action potential is described in the literature as being an "all-or-nothing" event, such that once the activation threshold voltage of a neuron is reached at the beginning of the axon, then the action potential will continue the entire length of a healthy axon without stopping. This phenomenon is due to a regular spacing of voltage-gated ion channels present along the axon. The local positive membrane potential causes sodium (Na+)-specific, voltage-gated ion channels to open. Positively charged Na+ ions then flow down their concentration gradient into the cell to further depolarize the region. At sufficient membrane depolarization, potassium (K+)-specific voltage-gated ion channels open, causing positively charged K+ to flow out of the cell, allowing regions at the beginning of the axon to return to resting potential. Through this mechanism, positive potential will travel the length of the axon to the axon terminal. These steps are further illustrated in Figure 3.

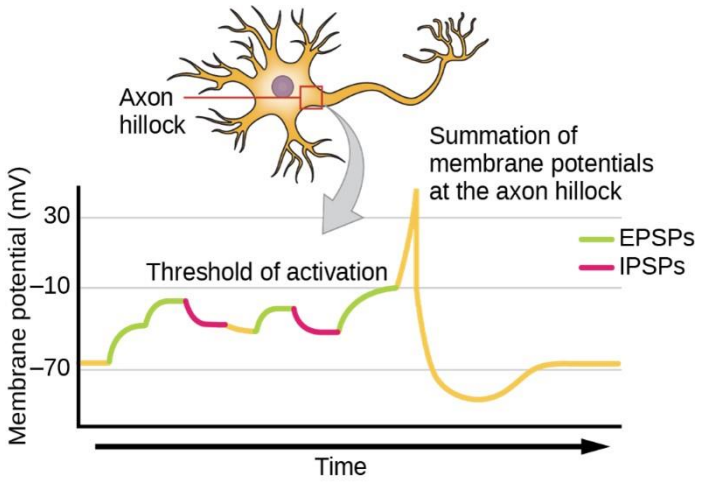

Figure 2. Neurons can receive both excitatory and inhibitory postsynaptic potentials. These signals summate at the axon hillock. If the voltage threshold is reached, an action potential is launched (Rye et al. 2024).

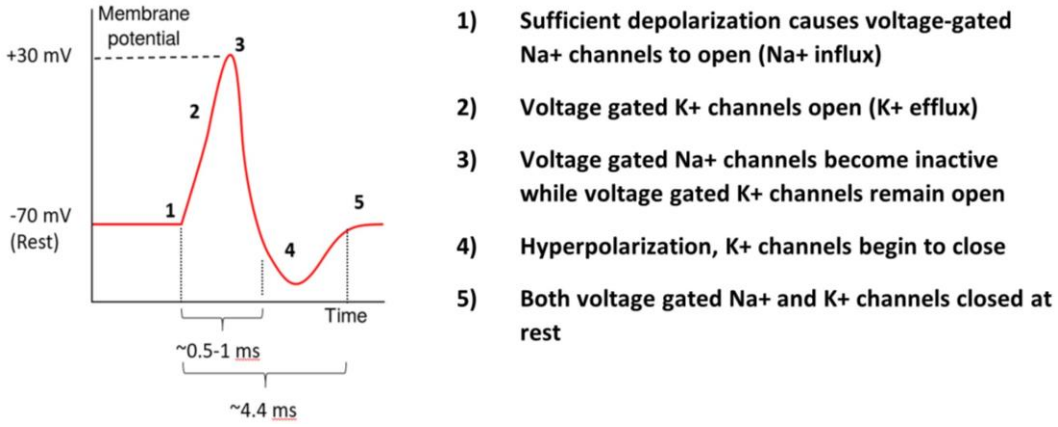

Figure 3. Voltage gated Na+ and K+ channels drive action potential firing down the axon and each will activate at different voltage thresholds. When voltage-gated Na+ channels open, Na+ ions will flow down their concentration gradient into the cell, while voltage-gated K+ channel activation causes K+ ions to flow down their concentration gradient out of the cell.

The Hodgkin–Huxley computational model quantitatively estimates current density in a neuron as an action potential moves down the axon. It was derived in the 1950s from experiments in a giant squid axon and famously is used for describing the electrochemical physiology of neurons. The model approximates the axon as a circuit with the cell membrane acting as a capacitor and the ion channels as resistors. Any current density across the membrane will either add to the capacitance of the membrane or leak out through ion channels as described in Equation 1, where I_M is the current density across the membrane, C_M is the membrane capacitance, V is the membrane voltage, t is time, and I_i is the current density across a given ion channel i.

$$I_M = C_M\left(\frac{\partial V}{\partial t}\right) + \sum_i I_i(t) \ . \qquad (1)$$

In the original model, the three types of ion channels considered were Na+ channels, K+ channels, and passively open leak (L) channels. The second term from Equation 1 above can therefore be written as Equation 2, where g is the conductance of a given ion channel and E is the reversal potential of a given ion channel. Terms m, n, and h in Equation 2 are dimensionless gating terms between 0 and 1 that describe the activation of a given ion channel, with m being Na+ channel activation, h being Na+ channel inactivation, and n being K+ channel activation. The reversal potential of a channel is the membrane potential at which ion flux across the membrane is 0 and is given by Equation 3, where R is the ideal gas constant, T is temperature in kelvin, z is the ion charge, F is the Faraday constant, and *conc* is ion concentration either outside or inside the cell.

$$\sum_i I_i(t) = g_L(V - E_L) + g_{Na}m^3h(V - E_{Na}) + g_k n^4(V - E_k)\,. \quad (2)$$

$$E_i = \frac{R\mathrm{T}}{z\mathrm{F}} * ln\left(\frac{conc_{out}}{conc_{in}}\right). \quad (3)$$

1.2 Limitations to Classic Hodgkin–Huxley Model

While the Hodgkin–Huxley computational model is a fair approximation of the electrophysiology of a neuron, there are some key limitations to the model that should be considered for the purposes of this review investigating the effects of acoustic signal in the brain. In addition to the electrochemical response, there are also thermodynamic changes to a neuron during the firing of an action potential that are not described by the Hodgkin–Huxley model (Cohen 1973). For instance, it has been shown that the axonal radius becomes thicker in the local region where the action potential is at its peak and that the axon's length shortens during firing (El Hady and Matcha 2015). Additionally, there are thermal changes to the neuron where heat is given off and then reabsorbed following action potential firing (Tasaki et al. 1989). It is unknown whether these mechanical changes to the neuron provide feedback to influence the action potential propagation.

The Hodgkin–Huxley model is also limited in the number of ion channel types accounted for that influence neuronal firing. There are many more ion channels known to exist in the CNS. Of particular interest to this review are mechanically gated ion channels such as TRPV1, TRPV2, TRPV4, Piezo1, TRPC1, TRPM7 and the TRPP1/2 complex (Yoo et al. 2022). It is hypothesized that ultrasound can act on these ion channels to cause changes in neuronal activity. Ultrasound having the capability to initiate neuromodulation (Blackmore et al. 2019) suggests that the above-mentioned limitations to the classic Hodgkin–Huxley electrochemical understanding of the nervous system are significant. A more complete computational model of neural activation including mechanical and thermodynamic influence is still under investigation within the scientific community at large.

2. Transcranial Ultrasound Neuromodulation

In recent years, transcranial focused ultrasound (tFUS) shows promise to be a safe and effective method for delivering neuromodulation to animal and human subjects. The constructive interference of incident pressure waves allows directivity of the ultrasound beam to be focused at any desired depth without impacting surface layer or neighboring tissues (Haar 1999; Blackmore et al. 2019). Traditionally,

tFUS has been employed clinically at high intensities (~1000 W/cm^2) to noninvasively destroy malignant tissue through thermal ablation (Fry et al. 1954). However, more recent advancements indicate that low-intensity ultrasound (30–500 mW/cm^2) (Tyler 2011) is sufficient to modulate neural activity with negligible heating or damage to tissue (Tufail et al. 2010; Yoo et al. 2011; Mueller et al. 2016; Lin et al. 2019). Fry et al. (1958) was one of the first research groups to demonstrate the reversible effects of low-intensity ultrasound by inhibiting visual evoked potentials in a cat brain. Since then, the literature has become rich with studies suggesting that differing ultrasound parameters can provide the versatility of both excitatory and inhibitory behavioral responses (Blackmore et al. 2019).

Although the exact mechanism for how ultrasound modulates neurons is still debated and under investigation, there is ample evidence that tFUS is clinically valuable. Lasting therapeutic effects from neural stimulation are thought to act on neural connections similar to how synaptic plasticity occurs in the hippocampus during learning and memory consolidation (Polanía et al. 2018). One protein that aids in the potentiation or depression of synapses related to synaptic plasticity is brain-derived neurotrophic factor (BDNF) (Lu 2003). Tufail et al. observed that tFUS increased secretion of BDNF following sonication of the hippocampus, suggesting that tFUS has the potential to provide long-term plastic changes to neural circuits (Tufail et al. 2010). Another study observed that rodents receiving tFUS exhibited increased levels of the extracellular neurotransmitters dopamine and serotonin up to 2 h following stimulation as compared with controls. These findings are promising since both dopamine and serotonin are related to mood regulation and are directly implicated in neurological disorders such as Parkinson disease and depression. Even more interesting is that neurotransmitter analysis was sampled from the frontal lobe while sonication was focused deeper in the brain at the thalamus (Min et al. 2011). These results indicate tFUS has the potential to have long-term therapeutic benefit both locally and downstream of the targeted neural network.

2.1 Theories of Mechanisms of Action for Ultrasound Neuromodulation

Tyler et al. (2008) showed that ultrasound acts at the molecular level of neuronal firing. The ultrasound pulse affects the gating kinetics of voltage-gated ion channels that ultimately leads to increased transient ion release, action potential firing, and synaptic neurotransmitter release (Tyler et al. 2008). Although a robust finding, the exact mechanism for how ultrasound modulates cells in the CNS remains poorly understood and highly debated within the scientific community. Two competing hypotheses for mechanisms of action are cavitation and acoustic radiation force.

Cavitation is when pressure oscillations cause pockets of dissolved gas to form bubbles either within or near the membrane of a cell. These gas bubbles would oscillate at the acoustic carrier frequency, potentially causing pores to form in the membrane bilayer or causing changes to the capacitance of the membrane by changing the distance between intra- and extracellular layers. In contrast, acoustic radiation force is defined as the integration of the displacement of the cell membrane over time due to a transfer of momentum by a passing acoustic wave.

There is some recent evidence against the cavitation theory. First, there is not much dissolved gas present in the brain compared to other areas of the body such as the lung or stomach. However, if cavitation was still the leading mechanism for bioeffects from ultrasound, then one would expect the success rate of neuronal firing to increase with an increase in gas deposition in the environment. In one study, neural responses to ultrasound in gassed versus degassed media were tested with no observable difference between the two. Furthermore, no bubble formation was observed using a camera resolution of 532 nm (Yoo et al. 2022). At higher frequencies greater than 1 MHz, the efficiency for cavitation to occur significantly decreases (Tyler 2011; Nguyen et al. 2017). However, there are multiple studies suggesting that ultrasound can generate reversible activation of neurons at significantly higher frequencies on the order of tens of megahertz (Menz 2013), with one study suggesting action potential generation in salamander retina using ultrasound at 43 MHz (Lin 2019).

By systematically blocking specific ion channels from opening, Yoo et al. (2022) isolated the mechanically gated ion channels that responded to ultrasound, thereby supporting the theory for acoustic radiation force being the main mechanism for ultrasound neuromodulation. The study suggests that a transfer of momentum applies tension onto the lipid bilayer of a neuron cell membrane from a passing ultrasound pulse. Transient receptor potential (TRP) and Piezo1 nonspecific cation channels then open with some probability due to mechanical gating, causing calcium (Ca^{2+}) to flow down its concentration gradient into the neuron. After approximately 200 ms, intracellular Ca^{2+} concentration reaches about 3 μM, allowing enough Ca^{2+} to bind to chemically gated cation channels such as TRPM4 and T-type Ca^{2+} channels. Na^{+} and Ca^{2+} flood into the cell, significantly depolarizing the neuron and launching an action potential via voltage-gated ion channels, as described in Section 1.1. Figure 4 depicts this proposed chain of events (Yoo et al. 2022).

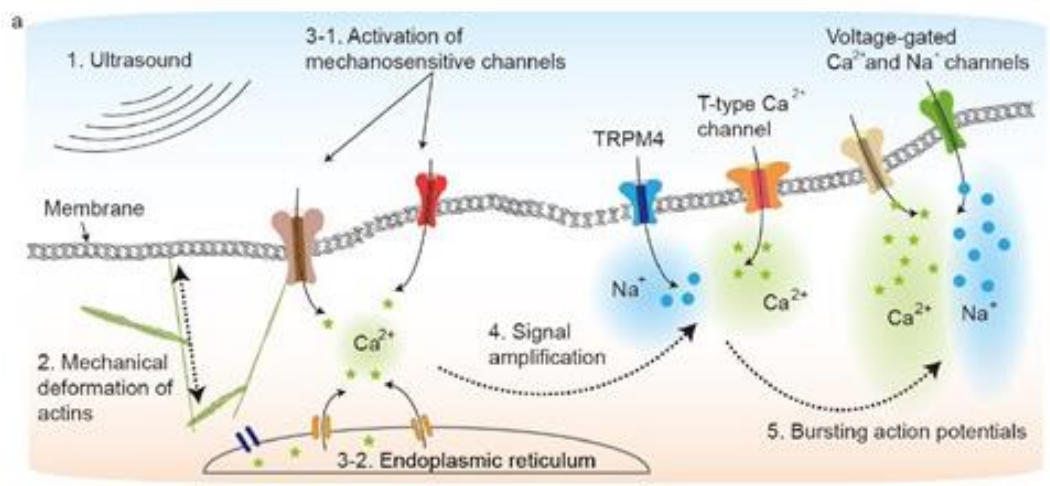

Figure 4. The molecular pathway activated by ultrasound (reproduced from Yoo et al. 2022).

The same group evidenced the importance of extracellular Ca^{2+} present for neurons to be modulated by ultrasound. Voltage was measured in neurons exposed to media with and without Ca^{2+}. Only those neurons in media containing Ca^{2+} showed a significant change in voltage, suggesting that the direct influx of Ca^{2+} into neurons drives the mechanism for ultrasound neuromodulation (Yoo et al. 2022).

Translating the results from this study into an effective computational model predicting ultrasound neuromodulation still requires some investigation. Some questions to explore include how much tension is required to activate TRP and Piezo1 mechanically gated ion channels, what is the rate of Ca^{2+} influx and at what rate is it cleared from the cell following ultrasound application, and what is the conductance of Ca^{2+}-gated channels? Furthermore, there are also Ca^{2+}-gated, K^{+}-specific ion channels on the lipid bilayer (Kshatri et al. 2018; Chen et al. 2022). If the ultrasound signal stops before cascading depolarization occurs, will the transient increase of intracellular Ca^{2+} result in a K^{+} efflux that will ultimately hyperpolarize the cell and inhibit cell firing? This component, though speculative, could lead to defining appropriate pulse repetition frequency to result in stimulation or inhibition of a neuron.

2.2 Limitations of tFUS

One of the main limitations of tFUS is that the human skull acts as a low-pass filter due to the high acoustic impedance of bone relative to soft tissue. When transmitting ultrasound across the skull, higher frequencies are reflected and attenuated within the bone, making it difficult to track the acoustic signal being absorbed within the brain. Studies show that an optimal frequency range for adequate transmission through the skull and coupling with neural tissue is 0.44–

0.67 MHz (Tyler et al. 2008). These low frequencies predict a subcentimeter spatial resolution as given by Equation 4, where λ is wavelength, v is acoustic velocity, and f is acoustic frequency. Since the velocity of acoustic waves in neural tissue is approximately 1550 m/s (Goss et al. 1978), a focal region of 2.3–3.5 mm can be predicted when using the above optimal low-frequency range for transcranial acoustic transmission.

$$\lambda = \frac{v}{f} . \tag{4}$$

A second limitation to tFUS was best exemplified by Legon et al. (2014), one of the first groups to perform successful tFUS in humans. Transmission of ultrasound across the skull showed a reduction of approximately four times the original spatial-peak pulse-average intensity. In 2018, the same group found a six-sevenfold decrease in acoustic pressure across the skull, suggesting that varying skull geometry can have a significant impact on the coupling of acoustic energy to brain tissue. In addition to intensity attenuation, ultrasound propagation shape and path can be impacted by individual differences in skull anatomy due to the interaction of ultrasound with the skull during transmission (Legon et al. 2018).

2.3 Parameters Required for Successful Transcranial Ultrasound Neuromodulation in Humans

An in-depth review of ultrasound parameters used for transcranial neuromodulation in humans where the transducers are in direct contact with the head via a coupling gel is provided in Biase et al. (2019). This section summarizes some of the necessary parameters for tFUS, including pressure, intensity, and frequency.

Reviews from the literature suggest that 0.2–2 MPa of pressure is necessary to modulate neurons in the CNS (Wang et al. 2020). If the lower bound of this range is considered, the corresponding acoustic intensity required is approximately 2.6 W/cm^2 following Equation 5, where I is acoustic intensity, p is acoustic pressure, ρ is density, and v is the longitudinal speed of sound. The product of density and acoustic velocity is the acoustic impedance, which is approximately 1.54e6 Rayls in the brain.

$$I = \frac{p^2}{\rho v} . \tag{5}$$

Accounting for the approximately 6 dB drop of acoustic intensity as signal passes through the skull (Legon et al. 2014), a minimum of approximately 10.35 W/cm^2 would need to be delivered outside of the human cranium to deliver 0.2 MPa of acoustic pressure to the outer cortex of the brain.

The ideal frequency range for ultrasound to transmit through the skull and couple to neural tissue is 0.44–0.67 MHz (Tyler et al. 2008; Biase et al. 2019; Wang et al. 2020). Longer wavelengths of lower frequency ultrasound would be harder to focus within the brain mass, requiring larger doses for the same level of impact. However, early studies of low-frequency ultrasound less than 300 kHz suggest increased occurrence of cerebral hemorrhage and tissue necrosis (Daffertshofer et al. 2005; Schneider et al. 2006; Ahmadi et al. 2012).

3. Thermoacoustic Neuromodulation

3.1 A Thermoacoustic Approach as an Alternative to Transcranial Application

An alternative, noncontact method of delivering ultrasound to a medium such as the brain is by using an RF source and inducing the thermoelastic effect. The skull is relatively transparent to electromagnetic waves at frequencies below 10 GHz (Andreuccetti et al. 1997), allowing an RF source to transmit signal past the scalp and skull to the underlying soft tissue of the brain. RFs are more readily absorbed in the brain than they are in bone, resulting in an instantaneous heating and thermoelastic expansion of brain matter. The mechanical deformation of tissue then launches a pressure wave with an initial pressure related to Equation 6, where μ_a is the RF absorption coefficient and F is the RF energy density, sometimes referred to as fluence.

$$p_0 = \Gamma \mu_a F \, . \tag{6}$$

The Grüneisen parameter Γ is a dimensionless term specific to a given material that describes how volume expansion will impact the resulting vibrations. It is calculated by Equation 7, where a is the material's linear thermal expansion coefficient, v is the acoustic velocity, and C_p is the heat capacity. Values from the literature of each of these parameters in brain tissue are given in Table 2.

$$\Gamma = \frac{3av^2}{C_p} \, . \tag{7}$$

Table 2. Values from the literature used to calculate the Grüneisen parameter in brain tissue. a assumes a physiologically relevant temperature range of 37–40 °C (Dagro et al. 2021). v is from Chen and Ostoja-Starzewski (2010) and C_p is from Hasgall (2018).

	a (1/°C)	v (m/s)	C_p (J/kg/°C)
Value to calculate Grüneisen parameter in brain tissue	1.37e-3	1450	3700

The pressure wave then propagates away from the acoustic source following Equation 8.

$$\nabla^2 p(r,t) - \frac{1}{v^2}\frac{\partial^2 p(r,t)}{\partial \mathrm{t}^2} = p_0 \,. \tag{8}$$

The generated ultrasound pulse is broadband as determined by a convolution between the RF pulse envelope and the impulse response of the tissue. In theory, the presence of higher frequencies in tissue using the thermoacoustic method could allow for improved focusing capability of the ultrasound signal as compared with tFUS.

3.2 Source Amplitude Required for Thermoacoustic Neuromodulation

This section calculates approximately how much RF energy density is required to generate enough ultrasound pressure in the brain to induce neuromodulation. These values are then compared with the Institute of Electrical and Electronics Engineers (IEEE) safety standard for reference (2006). Calculations were made of RF sources operating at carrier frequencies between 1 and 10 GHz. Carrier frequencies larger than 10 GHz would likely result in all the RF signal absorbing in the skull region before transmitting fully into the brain, as shown in Figure 5 where attenuation coefficients from a layered skull/brain system are plotted using values from the literature (Andreuccetti et al. 1997). Here the skull region is shaded grey and is assumed to be approximately 6 mm. The brain region is shaded white. Penetration depth is defined as the distance at which RF signal has decayed to 1/e or 37% of its initial amplitude, which is where the Y-axis begins. 1-GHz RF will reach its penetration depth at approximately 43 mm, which is about halfway through the brain mass, while 10 GHz will likely absorb almost entirely before reaching the brain mass.

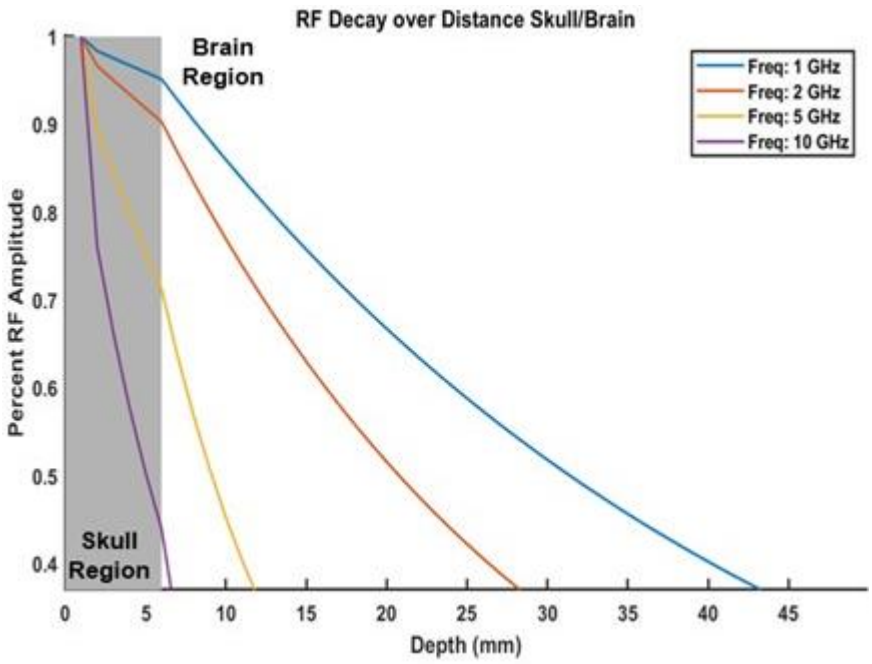

Figure 5. RF decay over distance as determined by attenuation coefficients from Andreuccetti et al. (1997), not accounting for additional losses of RF absorption in the scalp, cerebrospinal fluid, or other impeding structures.

The lower bound for acoustic pressure necessary to modulate neurons is 0.2 MPa (Wang et al. 2020). Using Equation 6, 0.2 MPa can be substituted in for p_0, 2.34 can be used for the Grüneisen parameter (Γ) of neural tissue as calculated from the values in Table 2, and the RF absorption coefficient at varying frequencies can be substituted in for μ_a using the values plotted in Figure 6 (Andreuccetti et al. 1997). The resulting energy density (F) required at varying carrier frequencies to generate the lower bound of neuromodulation on the surface of the brain is plotted in Figure 7, with densities varying between 50 and 450 mJ/cm^2.

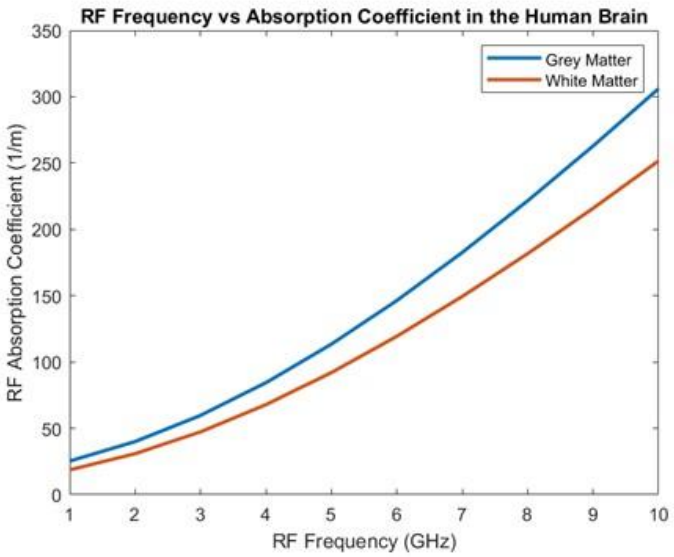

Figure 6. RF absorption coefficients (μ_a) in grey and white matter between 1 and 10 GHz (Andreuccetti et al. 1997).

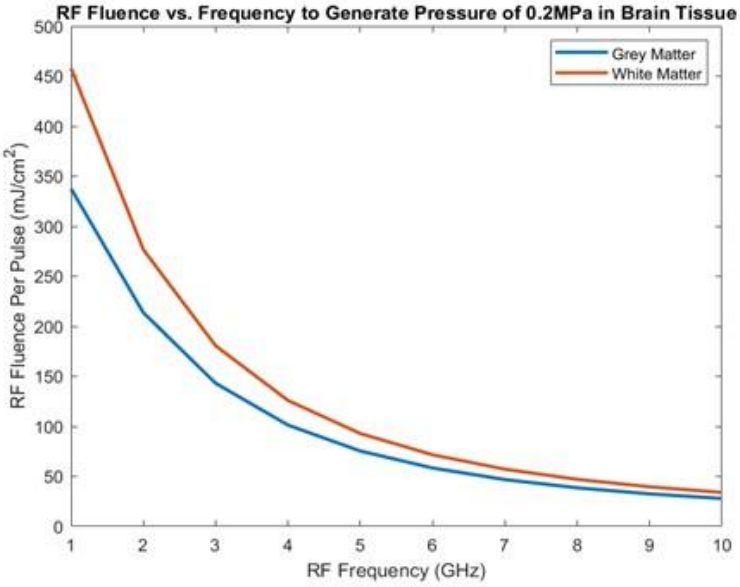

Figure 7. RF energy density required to generate lower bound for neuromodulation on the surface of the brain (0.2 MPa).

To put these required RF fluence values into perspective, let us compare them with the IEEE safety standards for maximum peak exposure from pulsed RF (IEEE 2006). The standard states that peak RF must be $< T^{\frac{1}{2}}$ kJ/m^2, where T is the pulse width of the RF source. To determine max permissible peak exposure, we must first define the necessary pulse widths required. To effectively convert electromagnetic energy into acoustic energy, the pulse width of the RF source must be less than the

time scale for stress to transmit away from the radiated area (τ_s), a condition referred to as stress confinement. This value can be calculated from Equation 9 (Xu and Wang 2006), where L_p is the characteristic linear dimension of the tissue volume and v is the acoustic velocity in tissue. Due to the high energy densities required for neuromodulation, it can be assumed that large antennas would be necessary. Axial heat diffusion would dominate in that the penetration depth of RF energy would be significantly less than the spot size. In this case, $L_p = \mu_a^{-1}$ (McKenzie 1990) and the stress confinement condition can be calculated as a function of RF carrier frequency, as shown in Figure 8 using the same RF absorption coefficients listed above. Stress confinement times between 1 and 10 GHz vary between approximately 5 and 35 μs. Figure 8 shows the use of these pulse widths to calculate maximum allowable peak RF exposures between 1 and 10 GHz, which varies between approximately 0.6 and 0.15 mJ/cm^2.

$$\tau_s = \frac{L_p}{v} \ . \tag{9}$$

Comparing Figures 7 and 8, the maximum peak exposure safety standard recommended while meeting the stress confinement condition in neural tissue is approximately 4 orders of magnitude lower than the required energy density to generate the lower bound of pressures required for neural modulation at the surface of the brain.

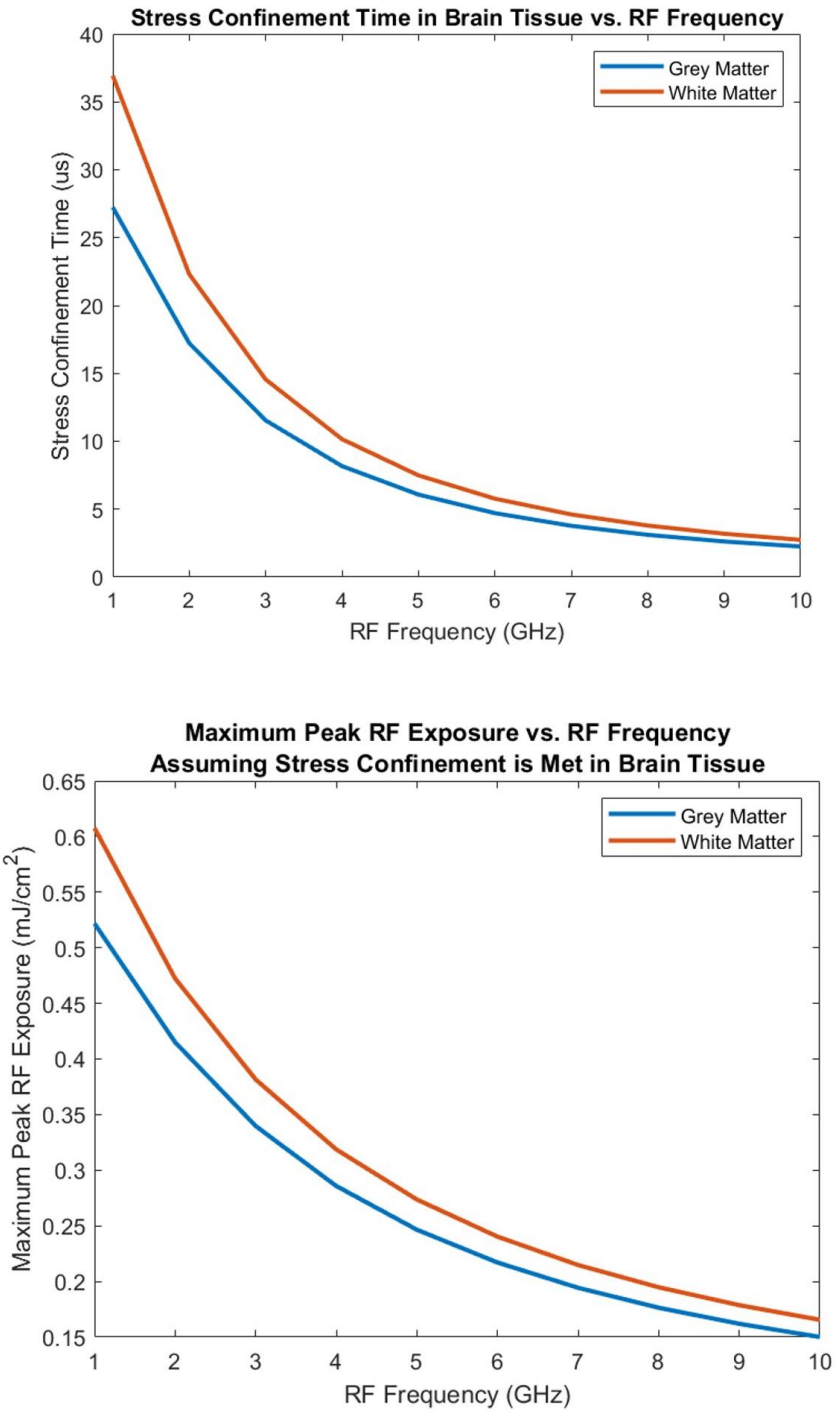

Figure 8. Top: stress confinement time in brain tissue for effective conversion of RF to acoustic signal using Equation 9 assuming $L_p = \mu_a^{-1}$ and an acoustic velocity of 1450 m/s. Bottom: the maximum peak exposure for RF in the brain following IEEE safety standard and assuming pulse width equals stress confinement times.

3.3 Beamforming

A 2D finite-difference acoustic simulator based on equations from Ottaviani (1971) and Kelly (1976) has been developed at Massachusetts Institute of Technology Lincoln Laboratory. A simple simulation placing acoustic sources along the inside curved surface of a skull (Figure 9) suggests that acoustic signal can be focused to a single location in the brain as determined by varying geometry of the skull.

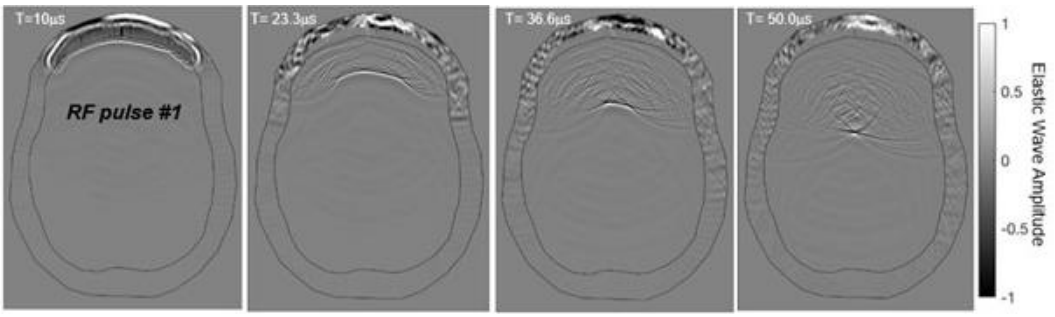

Figure 9. 2D finite-difference acoustic simulator suggesting that the curvature of the skull can act as a waveguide to focus ultrasound signal to a single focal location.

This section analytically assesses the feasibility of generating neuromodulatory pressures at a focal location at depth in the brain while spreading the RF source energy out over a larger area of the entire head so the amount of necessary RF energy density required is lower than the calculation in the previous section. In this example, an arbitrary spatial resolution of 1 mm is assumed at depth, which corresponds to an acoustic frequency of 1 MHz as given by Equation 4. The lower bound of pressure required for neuromodulation is again considered.

Substituting 0.2 MPa in for pressure and 1.54e6 Rayls for the acoustic impedance of brain tissue in Equation 5, an acoustic intensity of 2.6e4 W/m^2 is found to be the minimum acoustic intensity necessary to produce neuromodulation. Assuming a spherical surface area of the focal location ($4\pi r^2$) with radius 0.5 mm, this means a minimum of 0.08 W of total power would need to be delivered to the head mass. Let us further assume all 0.08 W is distributed over the entire hemisphere of the human head ($3\pi r^2$) where the average radius is 0.09 m. We can then substitute these values into Equation 5 again to calculate the amount of initial pressure that would need to be generated at the surface of the entire brain, as shown in Equation 10.

$$\frac{0.08[W]}{3\pi 0.09^2\ [m^2]} = \frac{p^2\ [Pa]}{1.56e6\ [Rayls]} \tag{10}$$

Solving gives 1278.6 Pa of initial pressure generated along the entire hemisphere of the surface of the brain that would then be focused to a location at depth. Generating this amount of pressure on the surface of the brain is much easier to

achieve with lower RF energy density than the previously assumed 0.2 MPa. The required RF energy densities to generate 1278.6 Pa are plotted in Figure 10 against frequency using the standard thermoelastic Equation 6 and the same values for the Grüneisen parameter and RF absorption coefficients assumed for the calculation of Figure 7. Comparing Figures 7 and 10, focusing acoustic signal to a 1-mm-diameter location could decrease the necessary RF fluence by 3 orders of magnitude down to between about 0.5 and 3 mJ/cm^2.

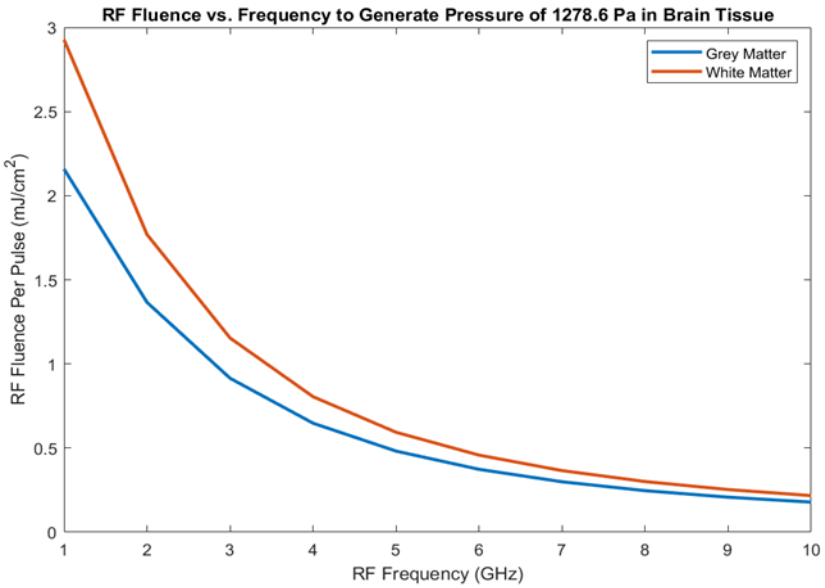

Figure 10. RF energy density required to generate 1278.6 Pa on the surface of the brain using Equation 6, RF absorption coefficients from Figure 7, and assuming a brain tissue Grüneisen parameter of 2.34 (as calculated from Table 2).

This example is theoretical and intended to show an ideal scenario based on a few key assumptions. One is that the geometry of a given individual's skull is the correct curvature to allow for such focusing. The other is that the RF signal hits the entire hemisphere of the head at the same time, which practically may not be feasible. This example also assumes an acoustic wave with a bandwidth up to 1 MHz is generated in the brain. Finally, this result depends strongly on the thermal expansion coefficient used to calculate the Grüneisen parameter. Reported values for this coefficient vary widely in the literature, often with different studies reporting values that are orders of magnitude different. However, the thermal expansion coefficient used in this report was determined for brain tissue at physiologically relevant temperatures, making it a fair value to consider (Dagro et al. 2021). Given all these assumptions, further experimental analysis of focusing thermoacoustic signal in the brain is required to verify this calculation.

4. Conclusion

This report reviews limitations to the classic electrochemical understanding of how neurons fire, particularly when considering that acoustic signals have been reported to cause reversible behavior changes in humans and animals. The report then considers the necessary parameters and conditions for two methods of delivering acoustic signal to the brain: one requiring direct contact of ultrasound transducers on the outside of the skull, and the other using RF sources to transmit signal through the skull and generate ultrasound in the brain via the thermoacoustic effect. Studies show that neuromodulation from ultrasound requires pressure levels on the order of MPa. While it is not difficult to apply these pressure levels to the brain via transcranial ultrasound contact transducers, it is a difficult level to achieve for the noncontact thermoacoustic case within the IEEE safety standards for peak RF exposure. One consideration explored in this review to reduce the necessary RF exposure levels is by generating lower pressures of ultrasound on the surface of the brain that focus down to a smaller region in the brain. While the RF exposure necessary for neuromodulation at depth was shown to be significantly reduced in this case, there were many assumptions that needed to be met, including the bandwidth of the thermoacoustic signal, geometry of the head, and thermoelastic properties of the neural tissue in a healthy physiological system. Experimental analysis is required to further verify the analytical outcomes of this report.

5. References

Ahmadi F, McLoughlin IV, Chauhan S, ter-Haar G. Bio-effects and safety of low-intensity, low-frequency ultrasonic exposure. Prog Biophys Mol Biol. 2012;108(3):119–138. https://doi.org/10.1016/j.pbiomolbio.2012.01.004

Andreuccetti D, Fossi R, Petrucci C. An internet resource for the calculation of the dielectric properties of body tissues in the frequency range 10 Hz – 100 GHz. Institute of Applied Physics Nello Carrara; c1997–2024. http://niremf.ifac.cnr.it/tissprop/

Biase LD, Falato E, Lazzaro VD. Transcranial focused ultrasound (tFUS) and transcranial unfocused ultrasound (tus) neuromodulation: from theoretical principles to stimulation practices. Front Neurol. 2019;10:549.

Blackmore J, Shrivastava S, Sallet J, Butler CR, Cleveland RO. Ultrasound neuromodulation: a review of results, mechanisms and safety. Ultrasound Med Biol. 2019;45(7):1509–1536.

Chen Y, Ostoja-Starzewski M. MRI-based finite element modeling of head trauma: spherically focusing shear waves. Acta Mechanica. 2010;213(1–2):155–167.

Chen S et al. A review of bioeffects induced by focused ultrasound combined with microbubbles on the neurovascular unit. J Cereb Blood Flow Metabol. 2022;42(1):3–26. https://doi.org/10.1177/0271678X211046129

Cohen LB. Changes in neuron structure during action potential propagation and synaptic transmission. Physiol Rev. 1973;53:373–418.

Daffertshofer M et al. Transcranial low-frequency ultrasound-mediated thrombolysis in brain ischemia: increased risk of hemorrhage with combined ultrasound and tissue plasminogen activator: results of a phase II clinical trial. Stroke. 2005;36(7):1441–1446.

Dagro AM, Li H, DiLeonardi AM, Hogan JD. Nonlinearity of the coefficient of thermal expansion in brain tissue. J Mech Behav Biomed Mater. 2021;123:104779.

El Hady A, Machta B. Mechanical surface waves accompany action potential propagation. Nat Commun. 2015:6:6697. https://doi.org/10.1038/ncomms7697

Fry FJ, Ades HW, Fry WJ. Production of reversible changes in the central nervous system by ultrasound. Science. 1958;127(3289):83–84.

Fry WJ, Mosberg WH, Barnard JW, Fry FJ. Production of focal destructive lesions in the central nervous system with ultrasound. J Neurosurg. 1954;11(5):471–478.

Goss SA, Johnston RL, Dunn F. Comprehensive compilation of empirical ultrasonic properties of mammalian tissues. J Acoust Soc Am. 1978;64(2):423–457.

Haar GT. Therapeutic ultrasound. Euro J Ultrasound. 1999;9(1):3–9.

Hasgall PA et al. IT'IS database for thermal and electromagnetic parameters of biological tissues, version 4.1. IT'IS Foundation; 2022 Feb 22. http://doi.org/10.13099/VIP21000-04-1

Hodgkin AL, Huxley AF. A quantitative description of membrane current and its application to conduction and excitation in nerve. J Physiol. 1952;117(4):500–544.

[IEEE] Institute of Electrical and Electronics Engineers. C95.1-2019 - IEEE standard for safety levels with respect to human exposure to radio frequency electromagnetic fields, 0 Hz to 300 GHz. IEEE; 2019. http://doi.org/10.1109/IEEESTD.2019.8859679

Kelly KR, Ward RW, Treitel S, Alford RM. Synthetic seismograms: A finite - difference approach. Geophysics. 1976;41(1):2–27.

Kshatri AS, Gonzalez-Hernandez A, Giraldez T. Physiological roles and therapeutic potential of Ca2+ activated potassium channels in the nervous system. Front Mol Neurosci. 2018;11:258.

Legon W, Ai L, Bansal P, Mueller JK. Neuromodulation with single element transcranial focused ultrasound in human thalamus. Hum Brain Mapp. 2018;39(5):1995–2006.

Legon W et al. Transcranial focused ultrasound modulates the activity of primary somatosensory cortex in humans. Nat Neurosci. 2014;17(2):322–329.

Liberman MC, Adams J. The peripheral auditory system. Fall 2005. Massachusetts Institute of Technology; 2005. https://ocw.mit.edu/courses/hst-721-the-peripheral-auditory-system-fall-2005/pages/

Lin Z et al. Ultrasound stimulation modulates voltage-gated potassium currents associated with action potential shape in hippocampal ca1 pyramidal neurons. Front Pharmacol. 2019;10:544.

Lu B. BDNF and activity-dependent synaptic modulation. Learn Mem. 2003;10(2):86–98.

McKenzie AL. Physics of thermal processes in laser-tissue interaction. Phys Med Biol. 1990;35(9):1175–1209.

Menz MD, Oralkan O, Khuri-Yakub PT, Baccus SA. Precise neural stimulation in the retina using focused ultrasound. J Neurosci. 2013;33(10):4550–4560.

Min B-K et al. Focused ultrasound modulates the level of cortical neurotransmitters: potential as a new functional brain mapping technique. Int J Imag Syst Technol. 2011;21(2):232–240.

Mueller JK, Ai L, Bansal P, Legon W. Computational exploration of wave propagation and heating from transcranial focused ultrasound for neuromodulation. J Neural Eng. 2016;13(5):056002.

Nguyen TT, Asakura Y, Koda S, Yasuda K. Dependence of cavitation, chemical effect, and mechanical effect thresholds on ultrasonic frequency. Ultrason Sonochem. 2017;39:301–306.

Ottaviani M. Elastic wave propagation in two evenly-welded quarter-spaces. Bull Seismol Soc Am. 1971;61:1119–1152.

Polanía R, Nitsche MA, Ruff CC. Studying and modifying brain function with non-invasive brain stimulation. Nat Neurosci. 2018;21(2):174–187.

Rye C et al. OpenStax: Biology 35.2 how neurons communicate. Rice University; c1999–2024 [accessed 2024 Feb 12]. https://openstax.org/books/biology/pages/35-2-how-neurons-communicate?query=axon+hillock&target=%7B%22index%22%3A0%2C%22type%22%3A%22search%22%7D#fs-idm98199488

Schneider F et al. Brain edema and intracerebral necrosis caused by transcranial low-frequency 20-kHz ultrasound: a safety study in rats. Stroke. 2006;37(5):1301–1306. https://doi.org/10.1161/01.STR.0000217329.16739.8f

Tasaki I, Kusano K, Byrne P. Rapid mechanical and thermal changes in the garfish olfactory nerve associated with a propagated impulse. Biophys J. 1989;55(6):1033–1040.

Tufail Y et al. Transcranial pulsed ultrasound stimulates intact brain circuits. Neuron. 2010;66(5):681–694.

Tyler WJ et al. Remote excitation of neuronal circuits using low-intensity, low-frequency ultrasound. PLoS One. 2008;3(10):e3511.

Tyler WJ. Noninvasive neuromodulation with ultrasound? A continuum mechanics hypothesis. Neuroscientist. 2011;17(1):25-36.

Vladišauskas A, Jakevičius L. Absorption of ultrasonic waves in air. Ultragarsas (Ultrasound). 2004;1(50):46–49.

Wang S et al. Ultrasonic neuromodulation and sonogenetics: a new era for neural modulation. Front Physiol. 2020;11:543198.

Xu M, Wang LV. Photoacoustic imaging in biomedicine. Rev Sci Instrum. 2006;77(4):041101. https://doi.org/10.1063/1.2195024

Yoo S, Mittelstein DR, Hurt RC, Lacroix J, Shapiro MG. Focused ultrasound excites cortical neurons via mechanosensitive calcium accumulation and ion channel amplification. Nat Commun. 2022;13(1):493. https://doi.org/10.1038/s41467-022-28040-1

Yoo S-S et al. Focused ultrasound modulates region specific brain activity. NeuroImage. 2011;56(3):1267–1275.

List of Symbols, Abbreviations, and Acronyms

2D	two-dimensional
BDNF	brain-derived neurotrophic factor
Ca^{2+}	calcium
CNS	central nervous system
IEEE	Institute of Electrical and Electronics Engineers
K+	potassium
Na+	sodium
RF	radio frequency
tFUS	transcranial focused ultrasound
TRP	transient receptor potential

Nomenclature

a	linear thermal expansion coefficient
conc	ion concentration
C_M	membrane capacitance
C_p	heat capacity
E	reversal potential
F	Faraday constant
F	RF energy density
f	acoustic frequency
Γ	Grüneisen parameter
g	conductance
h	sodium channel inactivation gating term
I	acoustic intensity
I_i	current density across a given ion channel i
I_M	current density across membrane

K	potassium
λ	wavelength
L	leak
L_p	characteristic linear dimension of tissue volume
μ_a	RF absorption coefficient
m	sodium channel activation gating term
n	potassium channel activation gating term
p	acoustic pressure
ρ	density
R	ideal gas constant
τ_s	stress confinement time
t	time
T	temperature
T	pulse width
V	voltage
v	acoustic velocity
z	ion charge

1 (PDF)	DEFENSE TECHNICAL INFORMATION CTR DTIC OCA
1 (PDF)	DEVCOM ARL FCDD RLB CI TECH LIB